

3D Cardiac Anatomy Generation Using Mesh Latent Diffusion Models

Jolanta Mozyrska^a, Marcel Beetz^b, Luke Melas-Kyriazi^c, Vicente Grau^b, Abhirup Banerjee^{b,d,1}, Alfonso Bueno-Orovio^{a,1,*}

^aDepartment of Computer Science, University of Oxford, Oxford, OX1 3QD, United Kingdom

^bInstitute of Biomedical Engineering, Department of Engineering Science, University of Oxford, Oxford, OX3 7DQ, United Kingdom

^cVisual Geometry Group, Department of Engineering Science, University of Oxford, Oxford, OX1 3PH, United Kingdom

^dDivision of Cardiovascular Medicine, Radcliffe Department of Medicine, University of Oxford, Oxford, OX3 9DU, United Kingdom

Abstract

Diffusion models have recently gained immense interest for their generative capabilities, specifically the high quality and diversity of the synthesized data. However, examples of their applications in 3D medical imaging are still scarce, especially in cardiology. Generating diverse realistic cardiac anatomies is crucial for applications such as *in silico* trials, electromechanical computer simulations, or data augmentations for machine learning models. In this work, we investigate the application of Latent Diffusion Models (LDMs) for generating 3D meshes of human cardiac anatomies. To this end, we propose a novel LDM architecture – MeshLDM. We apply the proposed model on a dataset of 3D meshes of left ventricular cardiac anatomies from patients with acute myocardial infarction and evaluate its performance in terms of both qualitative and quantitative clinical and 3D mesh reconstruction metrics. The proposed MeshLDM successfully captures characteristics of the cardiac shapes at end-diastolic (relaxation) and end-systolic (contraction) cardiac phases, generating meshes with a 2.4% difference in population mean compared to the gold standard.

Keywords: Cardiac imaging, generative artificial intelligence, geometric deep learning, latent diffusion model, virtual anatomy generation

1. Introduction

Diffusion models have recently attracted significant attention in the deep learning community and beyond due to their excellent generative capabilities, specifically the high quality and diversity of the produced data. Prominent examples of diffusion models generating 2D images from text include Stable Diffusion, built upon the work by Rombach et al. (2022), and Google’s Imagen (Saharia et al., 2022). Beyond 2D spaces, recent innovations like the MeshDiffusion model (Liu et al., 2023) have showcased their potential for generating 3D shapes like cars, chairs, and other common-life objects.

Lately, diffusion models have been applied to medical imaging as well. According to the first survey on diffusion models in medical imaging (Kazerouni et al., 2023), there has been an exponential growth in the number of publications with applications spanning from segmentation and anomaly detection to 2D and 3D image generation. Examples include Latent Diffusion Models (LDMs) (Rombach et al., 2022), which outperform generative adversarial network-based methods (Goodfellow et al., 2014) for generating class-conditional 2D chest X-ray images (Packhäuser et al., 2023). LDMs have also demonstrated the ability to generate realistic synthetic 3D brain images (Pinaya et al., 2022).

Building on this momentum, we aim to utilize LDMs for generating 3D meshes of cardiac anatomies. Such models can address the problem of limited annotated medical data for machine learning models. Existing studies such as (Chen et al., 2021a) on histology images have demonstrated that supplementing real samples with synthetic data

*Corresponding author.

Email address: alfonso.bueno@cs.ox.ac.uk (Alfonso Bueno-Orovio)

¹These authors share senior authorship.

enhances the classification performance. The generated synthetic data can also be applied for electrophysiological computer simulations for *in silico* trials (Li et al., 2022, 2024; Camps et al., 2024, 2025).

While mitigating the challenges of data scarcity, it is essential to ensure the diversity of generated medical data. Given that human cardiac anatomies exhibit significant variations between individuals, diverse representations are vital. Furthermore, different aspects of this diversity align with different diseases, enabling clinicians to make precise diagnoses and treatments. Thus, employing models that can capture the broad spectrum of data diversity is paramount. The variational autoencoder based Mesh VAE (Beetz et al., 2022) has previously been successful in modeling diverse cardiac anatomy. In this study, we investigate the following question: *can latent diffusion models be used for capturing anatomical variability and generating realistic 3D meshes of human left ventricles (LVs)?*

To this end, we introduce a novel architecture – MeshLDM – a latent diffusion model designed to generate 3D synthetic cardiac anatomy meshes. In this regard, our contributions include: (i) development of MeshLDM, a LDM architecture specifically designed for generating 3D meshes of cardiac anatomies; (ii) evaluation of MeshLDM’s abilities to generate 3D meshes of the human LV at both the end-diastolic (relaxation) and end-systolic (contraction) cardiac phases, using a dataset of patients with acute myocardial infarction; (iii) assessing MeshLDM’s ability to capture fine-detailed anatomical changes caused by cardiac disease, including changes in basal plane tilt, mid-cavity diameter, and elongation; and (iv) demonstration of MeshLDM’s capability to successfully learn characteristics of end-diastolic and end-systolic meshes, including differences in myocardial thickness. Altogether, and to the best of the authors’ knowledge, this represents the first study that leverages LDMs for generating 3D meshes of cardiac anatomies.

The rest of the article is organized as follows: in Section 2, we describe the architecture of the proposed MeshLDM and its training process. Next in Section 3, we present both qualitative and quantitative analyses of the generated meshes. Finally in Section 4, we discuss the results of our experiments, address their limitations, and propose future improvements and extensions.

2. Materials and methods

2.1. Overview

In this study, we introduce a novel architecture – MeshLDM – a latent diffusion model designed to generate 3D meshes of cardiac anatomies (Figures 1 and 2). We train and evaluate our model using a dataset initially designed for the study of post-myocardial infarction (MI) based on magnetic resonance imaging (MRI) (Beetz et al., 2022). It comprises of meshes representing human LVs, as detailed in Section 2.2. We describe the architecture of the proposed MeshLDM in Section 2.3 and explain the training process of the MeshLDM, in particular the autoencoder and the denoising model, in Section 2.4.

2.2. Dataset

We use the dataset as described in (Beetz et al., 2022) along with the same pre-processing steps.

The dataset consists of 1034 meshes of human LVs at the end-diastolic (ED) cardiac phase and 1034 meshes at the end-systolic (ES) phase (Corral Acero et al., 2022, 2024). The data was acquired from post-MI patients and includes both ST-elevation MI (STEMI) and non-ST-elevation MI (NSTEMI) patients. The acquired cine MR images were processed to obtain 3D surface meshes of the LVs (Lamata et al., 2014). We split the mesh dataset into approximately 70% training, 5% validation, and 25% test datasets. Before inputting the data into the MeshLDM model, we apply standardization (subtracting the mean and dividing by the standard deviation) to each mesh. Each mesh has the same number of consistently ordered vertices, allowing us to treat the vertex coordinates as a fixed-size feature vector. We standardize each coordinate (x, y, z) by subtracting the mean and dividing by the standard deviation computed across the training dataset.

We train two separate models – one for ED data and another for ES data. The meshes from ED and ES phases vary considerably in shape. If we naively combined the ED and ES datasets and trained a single model, it would attempt to learn an average representation of both cardiac phases, likely resulting in the generation of anatomically unrealistic shapes blending the ED and ES characteristics (e.g., a partially contracted ventricle with a large volume). Such shapes would lack clinical utility because they would not accurately represent either phase of the cardiac cycle.

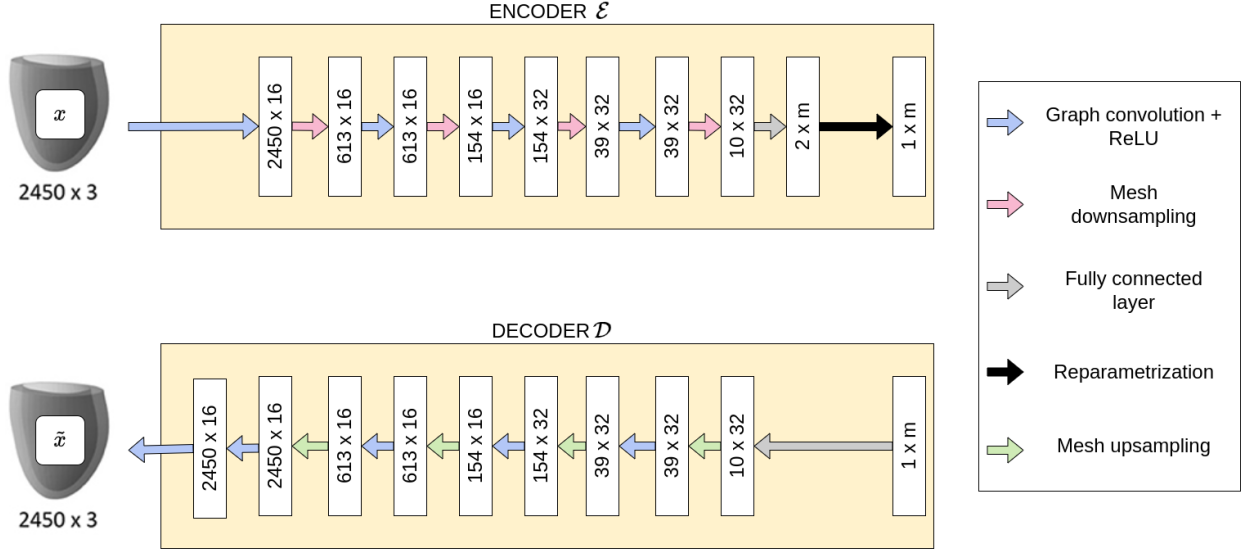


Figure 1: Illustration of the autoencoder part of the MeshLDM architecture.

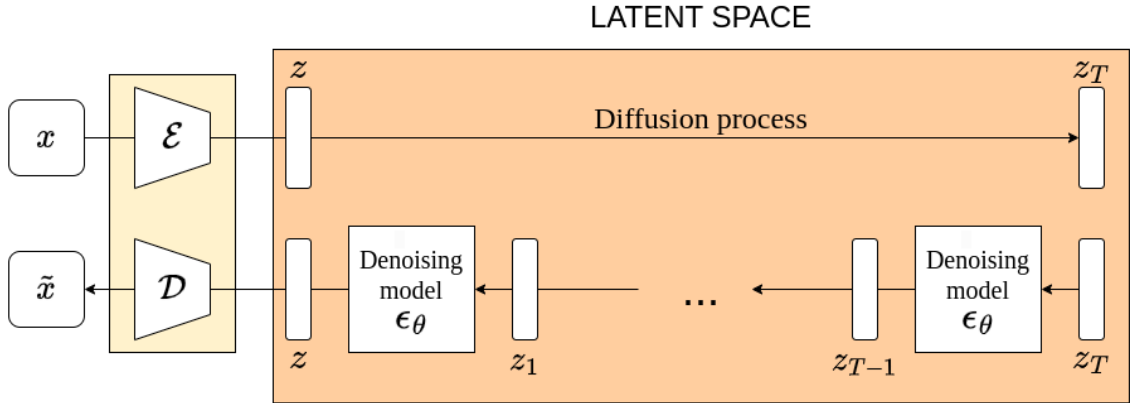


Figure 2: Illustration of MeshLDM architecture. It includes an autoencoder responsible for converting data to and from latent space and a denoising model, which performs the diffusion process.

2.3. MeshLDM architecture

The architecture of the proposed MeshLDM combines a Geometric Deep Learning (Bronstein et al., 2021) approach with latent diffusion models (Rombach et al., 2022). The model includes an autoencoder, responsible for converting 3D meshes to and from latent space, and a denoising model, which performs the diffusion process. The architecture of the model is presented in Figures 1 and 2.

2.3.1. Autoencoder

The autoencoder is based on the Mesh VAE architecture presented in (Beetz et al., 2022). It is designed to model ventricular anatomies utilizing a Geometric Deep Learning approach (Bronstein et al., 2021), namely graph convolutions and mesh pooling layers. An illustration of the autoencoder part of the MeshLDM architecture can be seen in Figure 1. The autoencoder allows us to map the input mesh to a latent space representation, capturing its anatomical structure in a compressed form. The dimension of the latent space, marked as m in Figure 1, is set to 16 in our experiments, following Beetz et al. (2022). In the training of the autoencoder, we employ Kullback-Leibler (KL)

regularization.

2.3.2. Denoising model

After encoding the entire dataset, we use it to train the denoising model. The denoising model learns to model the diffusion process in this latent space by progressively removing noise. The original LDM (Rombach et al., 2022) used an encoder to preserve the 2D data structure in image data and used a U-Net architecture as a denoising model. For our MeshLDM, we use a fully connected network as the denoising model. We employ 6 fully connected layers, with each layer having both input and output dimensions of 16. Between every pair of these layers, the Swish-1 activation function (Ramachandran et al., 2018) is applied. Additionally, at each layer, we add a diffusion timestep t encoded as a sinusoidal position embedding to the data, as described in (Ho et al., 2020). As our noise scheduler, we use the DDPM Scheduler introduced in (Ho et al., 2020) and implemented in the Diffusers library (von Platen et al., 2022), with steps = 1000, $\beta_0 = 0.0001$, and $\beta_T = 0.02$. Specifically, steps = 1000 means the diffusion process is discretized into 1000 timesteps. β_0 and β_T define the starting and ending values of the noise variance schedule. At each step, a small amount of Gaussian noise is added, with the noise level increasing from β_0 to β_T linearly across the 1000 steps. These values control how gradually the data is noised during the forward diffusion process.

2.4. Network training and implementation

2.4.1. Autoencoder

We first train the autoencoder component of the LDM. We use the same Mesh VAE architecture as proposed in (Beetz et al., 2022), where the dimension of the latent space is set to 16. We train the Mesh VAE using the same loss function for β -VAE framework and suggested parameters – the batch size of 8, Adam optimizer (Kingma and Ba, 2015) with a learning rate of 0.001, and 250 epochs. We train two separate models – one for ED data and one for ES data.

2.4.2. Denoising model

After training the autoencoder component of our MeshLDM, we use it to encode the training data into the latent space. Then, we normalize the obtained vectors, which become our training dataset for the denoising model. For training the denoising model we use the batch size of 64, the Adam optimizer, and a learning rate scheduler - LambdaLR from PyTorch framework (Paszke et al., 2019), initialized with a learning rate of 0.005.

We sample 1,000 random vectors (for each of the two models) from a normal distribution and input them into the trained denoising model. The resulting output vectors are scaled by the standard deviation and then shifted by the mean previously calculated during data normalization. Finally, we use the decoder to generate the corresponding synthetic 3D meshes.

2.5. Evaluation metrics

We evaluate the MeshLDM using several clinical and 3D metrics to assess its generative capabilities. We incorporate as clinical metrics the LV endocardial volume and LV myocardial mass. LV endocardial volume is the volume of inner cavity of the LV, whereas LV myocardial mass is calculated as the product of the LV myocardial volume (difference between LV epicardial and LV endocardial volumes) and the density of the myocardial tissue. The average density of the myocardium is assumed to be $\rho = 1.05$ g/mL (Beetz et al., 2022). These metrics are commonly used in clinical practice, making them a suitable choice for evaluating the realism of the generated samples.

We additionally evaluate the generated meshes using quantitative metrics commonly employed for assessing the quality of generated 3D structures (Yang et al., 2019; Peng et al., 2024). To this end, we convert the generated and reference (test dataset) meshes into point clouds by retaining only the vertices and removing the edges and faces. Let P_g denote the set of point clouds derived from the generated meshes, and let P_r represent the set of point clouds obtained from the reference meshes. When applying the point cloud metrics, we randomly select 285 meshes from the 1,000 generated meshes to ensure $|P_g| = |P_r|$. Here, $|P|$ denotes the number of point clouds in the dataset P. We use the following metrics:

Coverage (COV) (Achlioptas et al., 2018): For each point cloud in the generated set we first find the closest neighbor in the set of the reference point clouds. The Coverage score is the fraction of point clouds from reference set matched to at least one point cloud in the generated set. Formally, it is defined as:

$$\text{COV}(P_g, P_r) = \frac{\left| \left\{ \arg \min_{Y \in P_r} D(X, Y) \mid X \in P_g \right\} \right|}{|P_r|}, \quad (1)$$

where $D(X, Y)$ is distance between two point clouds.

Essentially, for each point cloud X in the generated set P_g , we find the closest point cloud Y in the reference set P_r based on a distance metric $D(X, Y)$. The $\arg \min_{Y \in P_r} D(X, Y)$ part identifies which reference point cloud is the closest to a given generated point cloud X , and hence the numerator $|\{\arg \min_{Y \in P_r} D(X, Y) \mid X \in P_g\}|$ counts the number of point clouds in the reference set that are matched to at least one point cloud in the generated set. Finally, dividing by $|P_r|$ yields the fraction of point clouds in the reference set that are matched to at least one point cloud in the generated set, measuring the coverage metric.

Minimum Matching Distance (MMD) (Achlioptas et al., 2018): For every point cloud Y from the reference dataset P_r , we calculate the distance to its nearest neighbor from the generated dataset P_g and then average the result. It is formally defined as follows:

$$\text{MMD}(P_g, P_r) = \frac{1}{|P_r|} \sum_{Y \in P_r} \min_{X \in P_g} D(X, Y). \quad (2)$$

1-Nearest Neighbor Accuracy (1-NNA): It was introduced by Lopez-Paz and Oquab (2017) and later adapted by Yang et al. (2019) for evaluating point cloud generative models. The 1-NNA measures the similarity between the generated and reference distributions. For each point cloud, we decide if it comes from the generated or reference dataset based on its nearest neighbor. A 1-NNA value closer to 50% indicates higher similarity between the distributions. Let $P_{-X} = P_r \cup P_g - \{X\}$ and N_X be the nearest neighbor of X in P_{-X} . Formally, 1-NNA is defined as follows:

$$\text{1-NNA}(P_g, P_r) = \frac{\sum_{X \in P_g} \mathbb{I}[N_X \in P_g] + \sum_{Y \in P_r} \mathbb{I}[N_Y \in P_r]}{|P_g| + |P_r|}, \quad (3)$$

where $\mathbb{I}[\cdot]$ is the indicator function.

In all cases, we use the Chamfer distance (CD) as the distance metric $D(\cdot)$:

$$\text{CD}(X, Y) = \sum_{x \in X} \min_{y \in Y} \|x - y\|_2^2 + \sum_{y \in Y} \min_{x \in X} \|x - y\|_2^2, \quad (4)$$

where X and Y are two point clouds with the same number of points. The chamfer distance from Equation (4) is used in Equation (3) to compute nearest neighbors between point clouds. Specifically, it is used to define the distance metric for determining N_X .

Additionally, we calculate the metrics for samples from the training dataset similar to Yang et al. (2019), and consider it as an upper bound since they come from the distribution that we target to simulate. We randomly select 285 samples from the training set and use them to compare the training and test set distributions.

3. Results

We conduct both qualitative and quantitative evaluations of the generated meshes, by comparing them to the gold standard, i.e., meshes in the test dataset.

3.1. Qualitative evaluation

We present 6 sample cases for each phase in Figure 3. We use two separate models, one trained on the ED data and the other on the ES data. Figure 3 does not present per-case correspondence between the meshes of those two cardiac phases. Similarly, the meshes in test dataset are also not in correspondence. Since we aim to generate



Figure 3: Sample meshes generated by MeshLDM ((a) end-diastole, (b) end-systole) and sample meshes from test dataset ((c) end-diastole, (d) end-systole).

new virtual meshes, not to reconstruct a given mesh based on a specific instance from the test dataset, pairwise comparisons between the generated and test meshes are not possible. We observe that the proposed MeshLDM successfully learns characteristics of the ED and ES meshes. The generated ED meshes have a larger overall volume and thinner myocardium than the ES meshes, which can also be observed in the meshes from the test dataset in Figure 3(c)-(d).

As shown in Figure 3(a)–(b), comparing meshes within a single row reveals notable anatomical diversity, including variations in the pointedness of the apex (e.g., meshes in row (b), columns 1–3) and differences in longitudinal curvature (e.g., meshes in row (a), columns 3–4). Additionally, the meshes generated by MeshLDM demonstrate diversity in terms of overall heart size, mid-cavity diameter, myocardial thickness, basal plane tilt, and left ventricular elongation. However, they present less diversity than the gold standard meshes in the test dataset, as further quantified next.

3.2. Evaluation of clinical metrics

We calculate clinical metrics, namely LV volume and LV mass, for each mesh and present their mean and standard deviation in Table 1. For comparison, we provide the same metrics for the meshes in the unseen test dataset, which we consider the gold standard in this study ($N = 285$).

We observe that MeshLDM can successfully capture the average shape of meshes for both cardiac phases, with the average difference in population mean across all scores at 2.4%. The mean LV volume and LV mass of the meshes in ED cardiac phase are very close to the ones from the gold standard, while the means in ES cardiac phase are slightly

Table 1: Clinical metrics achieved by MeshLDM and MeshVAE against gold standard (test dataset).

Phase	Metric	Gold standard [N=285]	MeshLDM [N=1,000]	Relative error MeshLDM	MeshVAE [N=1,000]	Relative error MeshVAE
ED	LV cavity volume (ml)	156.3 \pm 43.0	155.8 \pm 29.2	0.32%	162.6 \pm 44.7	4.03%
	LV mass (g)	123.0 \pm 30.6	123.1 \pm 17.6	0.08%	129.6 \pm 28.7	5.37%
ES	LV cavity volume (ml)	83.9 \pm 39.6	78.0 \pm 19.6	7.03%	84.6 \pm 28.5	0.83%
	LV mass (g)	130.7 \pm 33.9	126.9 \pm 18.0	2.09%	130.7 \pm 32.5	0%

Values represent mean \pm standard deviation.

Table 2: 3D metrics for meshes generated by MeshLDM and MeshVAE against training dataset. \uparrow : Higher values indicate better performance; \downarrow : Lower values indicate better performance.

Phase	Metric	Training set	MeshLDM	MeshVAE
ED	1-NNA (%)	49.48	63.46	62.06
	COV (% , \uparrow)	51.05	30.77	50
	MMD (mm, \downarrow)	12.86	13.05	12.54
ES	1-NNA (%)	49.13	72.20	59.44
	COV(% , \uparrow)	51.75	23.08	50.7
	MMD (mm, \downarrow)	13.48	14.83	12.96

higher. The standard deviations of the metrics in both cardiac phases are lower than the ones from the gold standard. This indicates that the MeshLDM can successfully learn the 3D shapes of the meshes, though the generated meshes represent less diversity than those from the gold standard.

3.3. Evaluation of cardiac structures generation

We compute several commonly used metrics, namely 1-NNA classifier, Coverage score, and Minimum Matching Distance, on the generated meshes and training dataset. The results are summarized in Table 2. As described in Section 2.5, the 1-NNA value should converge to 50% if the compared distributions are the same, as observed in our results between the training and gold standard test sets. The ED samples generated by MeshLDM achieve a value of approximately 63%, indicating a slight difference between the test and generated distributions while demonstrating a strong ability to accurately capture the variety of shapes observed in real patients’ data. The ES distribution reaches around 72% suggesting that features of ES shapes might be a bit more challenging to capture for the model. The Coverage score results indicate similar conclusions in terms of the difference between the generated and test distributions, as well as the lower performance for the ES phase. On the other hand, the minimum matching distance for the ED phase demonstrates that the generated structures are very similar to the gold standard distribution, with a difference of 13.05 mm, whereas the difference between the training set and test set is only slightly lower, at 12.86 mm.

3.4. Comparison with MeshVAE

To enable a meaningful comparison, we include results from the Mesh Variational Autoencoder (MeshVAE) model. This model was originally proposed by Beetz et al. (2022) for the modeling of ventricular anatomies, and

serves as the autoencoder part of our latent diffusion model.

In terms of clinical metrics, the relative errors of the means are lower for MeshLDM for the ED phase and lower for MeshVAE for the ES phase (Table 1). Meanwhile, the standard deviations produced by MeshVAE are closer to those of the gold standard than those produced by MeshLDM, indicating greater capabilities to capture diversity. This is also reflected in Table 2, with MeshVAE demonstrating a closer alignment with the training set in terms of coverage. However, the results of both methods are comparable for the rest of considered 3D metrics, especially in the case of MMD.

Altogether, MeshLDM proves to be a strong alternative to MeshVAE, though neither method consistently outperforms the other across all metrics.

4. Discussion

In this work, we have presented the first study investigating the application of LDMs for generating 3D meshes of cardiac anatomies. We have proposed a novel architecture, MeshLDM, which can generate realistic 3D meshes of LV cardiac anatomies, by combining a Geometric Deep Learning approach with diffusion models. The proposed model successfully captures the characteristics of 3D cardiac shapes and generates realistic 3D human left ventricles with only a 2.4% difference in population mean across all clinical evaluation metrics for both cardiac phases. The generated meshes exhibit variations in basal plane tilt, mid-cavity diameter, and shape elongation, though the overall diversity is relatively lower compared to the gold standard 3D meshes. This observation is consistent with clinical metrics and mesh generation quality, where standard deviations in both cardiac phases are lower than the ones from gold standard.

A potential solution to increase the diversity of the generated meshes would be to use a larger dataset. LDMs are known for their ability to generate diverse data, but this is only possible if the model is trained on a sufficiently large and diverse dataset. For example, Stable Diffusion was trained on LAION-400M (Schuhmann et al., 2021), a publicly available dataset of 400 million image-text pairs (Rombach et al., 2022), containing a wide variety of images and captions. In contrast, the dataset used in this study is relatively small and contains only 1,034 meshes of human left ventricles, which may have affected diversity of the generated meshes, though the size of our dataset is satisfactory in terms of post-MI 3D reconstruction.

One of the potential downstream applications of the proposed MeshLDM model is to apply it for generating synthetic cardiac structures for cardiac disease classification tasks (Suinesiaputra et al., 2017; Isensee et al., 2018; Bernard et al., 2018; Zhang et al., 2019; Avard et al., 2022; Corral Acero et al., 2022; Beetz et al., 2023a,c,d). In cardiology, 3D shape has been extensively studied to better understand and simulate the anatomy and function of both the healthy and diseased heart (Bai et al., 2015; Gilbert et al., 2019; Vincent et al., 2021). 3D-based biomarkers have also been shown to provide significant diagnostic value for a plethora of cardiovascular diseases, including MI (Suinesiaputra et al., 2017; Corral Acero et al., 2022). While traditional machine learning approaches to 3D cardiac shape analysis have primarily employed principal component analysis and related methods, more recent work has increasingly focused on deep learning techniques (Gilbert et al., 2020). While early deep learning approaches were based on grid-based representations of 3D shape (Qin et al., 2018; Xu et al., 2019; Biffi et al., 2020), newer studies have also explored geometric deep learning applied to both point cloud (Beetz et al., 2021, 2024; Peng et al., 2024; Seale et al., 2024) and mesh representations of the heart (Kong et al., 2021; Chen et al., 2021b; Beetz et al., 2023b; Meng et al., 2023; Kalaie et al., 2024). These existing approaches typically depend on large and high-quality cardiac data which is time-consuming, costly, and difficult to acquire. Our proposed MeshLDM can mitigate these challenges by synthesizing high-resolution, diverse, and realistic 3D cardiac structures. The generated synthetic data have valuable applications, including use in electrophysiological computer simulations for *in silico* trials (Li et al., 2024; Coleman et al., 2024; Dasí et al., 2024; Camps et al., 2025) and data augmentation for training cardiac disease classifiers (Beetz et al., 2023c; Corral Acero et al., 2022, 2024). However, demonstrating these downstream uses is well beyond the scope of this manuscript, as it would necessitate the development, training, and validation of new application-specific models and evaluation frameworks, each representing a significant research effort beyond the current study.

Our work is an important step towards exploring the possibilities of diffusion-based models in the field of medical imaging, especially 3D anatomy generation. As a future extension, a conditioning mechanism can be incorporated

in the MeshLDM that would allow us to generate data for specific subpopulations using the same model, instead of training separate models for different subgroups such as cardiac phases. Such a conditioning mechanism would enable, for instance, to train a single model on both ED and ES data. While incorporating a conditioning mechanism is a natural and promising extension, it was outside the scope of the current study. We focused on demonstrating the possibility of using latent diffusion models to generate realistic 3D cardiac anatomies for individual phases.

LV volume and mass are important clinical indicators of cardiac health, and LV volume is widely used in current clinical practice. Although they do not provide a detailed characterization of cardiac shapes, they help indicate whether the generated meshes fall within a plausible clinical range. As part of our future work, once the aforementioned conditioning mechanism enabling the correspondence between the ES and ED phases is implemented, further metrics such as LV ejection fraction could be computed to provide more comprehensive comparisons with established clinical metrics.

Further future work on the automatization process of cardiac mesh generation can also incorporate intermediate temporal phases (along with ED and ES phases) for the modeling of cardiac mechanics, as well as diverse demographic characteristics such as sex, age, body mass index, etc., towards subpopulation-specific cardiac anatomy modeling (Beetz et al., 2021).

5. Conclusion

In this study, we have introduced MeshLDM, a novel latent diffusion model architecture specifically designed for generating 3D meshes of human cardiac anatomies. Our extensive evaluations demonstrate that MeshLDM effectively captures the intricate characteristics of human cardiac anatomy at both end-diastolic and end-systolic phases across a wide range of clinical and 3D mesh reconstruction metrics, although with slightly less diversity compared to the clinical data. Nonetheless, our work represents a pioneering application of LDMs in 3D cardiac anatomy generation, offering a promising tool for addressing data scarcity in medical imaging and enhancing the realism and diversity of synthetic cardiac data. The successful implementation of MeshLDM underscores the potential impact of this and other generative models on advancing cardiac disease modeling, diagnosis, and treatment planning through high-fidelity virtual anatomy generation.

Conflict of Interest Statement

The authors declare that the research was conducted in the absence of any commercial or financial relationships that could be construed as a potential conflict of interest.

Author contributions

JM: Conceptualization, Formal Analysis, Investigation, Methodology, Software, Visualisation, Writing - original draft, Writing - review & editing. MB: Investigation, Data Curation, Writing - review & editing. LMK: Investigation, Writing - review & editing. VG: Investigation, Methodology, Project Administration, Data Curation, Writing - review & editing, Supervision. AB: Conceptualization, Investigation, Methodology, Project Administration, Writing - review & editing, Supervision, Funding acquisition. ABO: Conceptualization, Investigation, Methodology, Project Administration, Data Curation, Writing - review & editing, Supervision, Funding acquisition.

Funding

A. Banerjee holds a Royal Society University Research Fellowship (Grant No. URF\R1\221314). A. Bueno-Orovio acknowledges support from the Innovate UK grant 10110728.

Acknowledgments

This work made use of the University of Oxford's Advanced Research Computing (ARC) facility (<https://doi.org/10.5281/zenodo.22558>).

Code and data availability

The code is available at <https://github.com/mozyrska/Mesh-LDM>. The datasets used in this article is not publicly available due to ethical and legal restrictions related to patient confidentiality. Generated virtual data can be made available upon reasonable request.

References

- Achlioptas, P., Diamanti, O., Mitliagkas, I., Guibas, L., 2018. Learning representations and generative models for 3D point clouds, in: Dy, J., Krause, A. (Eds.), *Proceedings of the 35th International Conference on Machine Learning*, pp. 40–49. URL: <https://proceedings.mlr.press/v80/achlioptas18a.html>.
- Avard, E., Shiri, I., Hajianfar, G., Abdollahi, H., Kalantari, K.R., Houshmand, G., Kasani, K., Bitarafan-rajabi, A., Deevband, M.R., Oveisi, M., Zaidi, H., 2022. Non-contrast cine cardiac magnetic resonance image radiomics features and machine learning algorithms for myocardial infarction detection. *Computers in Biology and Medicine* 141, 105145.
- Bai, W., Shi, W., de Marvao, A., Dawes, T.J., O'Regan, D.P., Cook, S.A., Rueckert, D., 2015. A bi-ventricular cardiac atlas built from 1000+ high resolution MR images of healthy subjects and an analysis of shape and motion. *Medical Image Analysis* 26, 133–145.
- Beetz, M., Banerjee, A., Grau, V., 2021. Generating subpopulation-specific biventricular anatomy models using conditional point cloud variational autoencoders, in: *International Workshop on Statistical Atlases and Computational Models of the Heart*, pp. 75–83.
- Beetz, M., Banerjee, A., Grau, V., 2023a. Multi-objective point cloud autoencoders for explainable myocardial infarction prediction, in: *Medical Image Computing and Computer Assisted Intervention – MICCAI 2023*, Cham, pp. 532–542.
- Beetz, M., Banerjee, A., Grau, V., 2024. Modeling 3D cardiac contraction and relaxation with point cloud deformation networks. *IEEE Journal of Biomedical and Health Informatics* 28, 4810–4819.
- Beetz, M., Corral Acero, J., Banerjee, A., Eitel, I., Zacur, E., Lange, T., Stiermaier, T., Evertz, R., Backhaus, S.J., Thiele, H., Bueno-Orovio, A., Lamata, P., Schuster, A., Grau, V., 2022. Interpretable cardiac anatomy modeling using variational mesh autoencoders. *Frontiers in Cardiovascular Medicine* 9, 983868.
- Beetz, M., Corral Acero, J., Banerjee, A., Eitel, I., Zacur, E., Lange, T., et al., 2023b. Mesh U-Nets for 3D cardiac deformation modeling, in: *International Workshop on Statistical Atlases and Computational Models of the Heart*, pp. 245–257.
- Beetz, M., Corral Acero, J., Banerjee, A., Eitel, I., Zacur, E., Lange, T., et al., 2023c. Post-infarction risk prediction with mesh classification networks, in: *International Workshop on Statistical Atlases and Computational Models of the Heart*, pp. 291–301.
- Beetz, M., Yang, Y., Banerjee, A., Li, L., Grau, V., 2023d. 3D shape-based myocardial infarction prediction using point cloud classification networks, in: *2023 45th Annual International Conference of the IEEE Engineering in Medicine & Biology Society (EMBC)*, pp. 1–4.
- Bernard, O., Lalande, A., Zotti, C., Cervenansky, F., Yang, X., Pheng-Ann, H., 2018. Deep learning techniques for automatic MRI cardiac multi-structures segmentation and diagnosis: is the problem solved? *IEEE Transactions on Medical Imaging* 37, 2514–2525.
- Biffi, C., Cerrolaza, J.J., Tarroni, G., Bai, W., de Marvao, A., Oktay, O., et al., 2020. Explainable anatomical shape analysis through deep hierarchical generative models. *IEEE Transactions on Medical Imaging* 39, 2088–2099.

- Bronstein, M.M., Bruna, J., Cohen, T., Veličković, P., 2021. Geometric deep learning: Grids, groups, graphs, geodesics, and gauges *arXiv:2104.13478*. *arXiv: 2104.13478*.
- Camps, J., Berg, L.A., Wang, Z.J., Sebastian, R., Riebel, L.L., Doste, R., Zhou, X., Sachetto, R., Coleman, J., Lawson, B., Grau, V., Burrage, K., Bueno-Orovio, A., Weber dos Santos, R., Rodriguez, B., 2024. Digital twinning of the human ventricular activation sequence to clinical 12-lead ECGs and magnetic resonance imaging using realistic purkinje networks for in silico clinical trials. *Medical Image Analysis* 94, 103108.
- Camps, J., Wang, Z.J., Doste, R., Berg, L.A., Holmes, M., Lawson, B., Tomek, J., Burrage, K., Bueno-Orovio, A., Rodriguez, B., 2025. Harnessing 12-lead ECG and MRI data to personalise repolarisation profiles in cardiac digital twin models for enhanced virtual drug testing. *Medical Image Analysis* 100, 103361. URL: <https://www.sciencedirect.com/science/article/pii/S136184152400286X>.
- Chen, R.J., Lu, M.Y., Chen, T.Y., Williamson, D.F., Mahmood, F., 2021a. Synthetic data in machine learning for medicine and healthcare. *Nature Biomedical Engineering* 5, 493–497.
- Chen, X., Ravikumar, N., Xia, Y., Attar, R., Diaz-Pinto, A., Piechnik, S.K., Neubauer, S., Petersen, S.E., Frangi, A.F., 2021b. Shape registration with learned deformations for 3D shape reconstruction from sparse and incomplete point clouds. *Medical Image Analysis* 74, 102228.
- Coleman, J.A., Doste, R., Beltrami, M., Argirò, A., Coppini, R., Olivotto, I., Raman, B., 2024. Effects of ranolazine on the arrhythmic substrate in hypertrophic cardiomyopathy. *Frontiers in Pharmacology* 15, 1379236.
- Corral Acero, J., Lamata, P., Eitel, I., Zacur, E., Evertz, R., Lange, T., Backhaus, S.J., Stiermaier, T., Thiele, H., Bueno-Orovio, A., Schuster, A., Grau, V., 2024. Comprehensive characterization of cardiac contraction for improved post-infarction risk assessment. *Scientific Reports* 14, 8951.
- Corral Acero, J., Schuster, A., Zacur, E., Lange, T., Stiermaier, T., Backhaus, S.J., Thiele, H., Bueno-Orovio, A., Lamata, P., Eitel, I., Grau, V., 2022. Understanding and improving risk assessment after myocardial infarction using automated left ventricular shape analysis. *JACC: Cardiovascular Imaging* 15, 1563–1574.
- Dasí, A., Nagel, C., Pope, M.T., Wijesurendra, R.S., Betts, T.R., Sachetto, R., Loewe, A., Bueno-Orovio, A., Rodriguez, B., 2024. In Silico TRials guide optimal stratification of ATRial Fibrillation patients to Catheter Ablation and pharmacological medication: the i-STRATIFICATION study. *Europace* 26, euae150.
- Gilbert, K., Bai, W., Mauger, C., Medrano-Gracia, P., Suinesiaputra, A., Lee, A.M., Sanghvi, M.M., Aung, N., Piechnik, S.K., Neubauer, S., et al., 2019. Independent left ventricular morphometric atlases show consistent relationships with cardiovascular risk factors: a UK biobank study. *Scientific Reports* 9, 1130.
- Gilbert, K., Mauger, C., Young, A.A., Suinesiaputra, A., 2020. Artificial intelligence in cardiac imaging with statistical atlases of cardiac anatomy. *Frontiers in Cardiovascular Medicine* 7, 102.
- Goodfellow, I., Pouget-Abadie, J., Mirza, M., Xu, B., Warde-Farley, D., Ozair, S., Courville, A., Bengio, Y., 2014. Generative adversarial nets. *Advances in neural information processing systems* 27.
- Ho, J., Jain, A., Abbeel, P., 2020. Denoising diffusion probabilistic models, in: *Proceedings of the 34th International Conference on Neural Information Processing Systems*, Curran Associates Inc., Red Hook, NY, USA. pp. 6840–6851.
- Isensee, F., Jaeger, P.F., Full, P.M., Wolf, I., Engelhardt, S., Maier-Hein, K.H., 2018. Automatic cardiac disease assessment on cine-MRI via time-series segmentation and domain specific features, in: *International Workshop on Statistical Atlases and Computational Models of the Heart*, pp. 120–129.
- Kalaie, S., Bulpitt, A.J., Frangi, A.F., Gooya, A., 2024. A geometric deep learning framework for generation of virtual left ventricles as graphs, in: *Medical Imaging with Deep Learning*, pp. 426–443.

- Kazerouni, A., Aghdam, E.K., Heidari, M., Azad, R., Fayyaz, M., Hacıhaliloglu, I., Merhof, D., 2023. Diffusion models in medical imaging: A comprehensive survey. *Medical Image Analysis* 88, 102846. URL: <https://www.sciencedirect.com/science/article/pii/S1361841523001068>.
- Kingma, D.P., Ba, J., 2015. Adam: A method for stochastic optimization, in: 3rd International Conference on Learning Representations, ICLR 2015.
- Kong, F., Wilson, N., Shadden, S., 2021. A deep-learning approach for direct whole-heart mesh reconstruction. *Medical Image Analysis* 74, 102222.
- Lamata, P., Sinclair, M., Kerfoot, E., Lee, A., Crozier, A., Blazevic, B., Land, S., Lewandowski, A.J., Barber, D., Niederer, S., Smith, N., 2014. An automatic service for the personalization of ventricular cardiac meshes. *Journal of the Royal Society Interface* 11, 20131023.
- Li, L., Camps, J., Banerjee, A., Beetz, M., Rodriguez, B., Grau, V., 2022. Deep computational model for the inference of ventricular activation properties, in: International Workshop on Statistical Atlases and Computational Models of the Heart, pp. 369–380.
- Li, L., Camps, J., Jenny Wang, Z., Beetz, M., Banerjee, A., Rodriguez, B., Grau, V., 2024. Toward enabling cardiac digital twins of myocardial infarction using deep computational models for inverse inference. *IEEE Transactions on Medical Imaging* 43, 2466–2478.
- Liu, Z., Feng, Y., Black, M.J., Nowrouzezahrai, D., Paull, L., Liu, W., 2023. MeshDiffusion: Score-based generative 3D mesh modeling, in: 11th International Conference on Learning Representations, ICLR 2023.
- Lopez-Paz, D., Oquab, M., 2017. Revisiting classifier two-sample tests, in: 5th International Conference on Learning Representations, ICLR2017.
- Meng, Q., Bai, W., O'Regan, D.P., Rueckert, D., 2023. DeepMesh: Mesh-based cardiac motion tracking using deep learning. *IEEE Transactions on Medical Imaging* 43, 1489–1500.
- Packhäuser, K., Folle, L., Thamm, F., Maier, A., 2023. Generation of anonymous chest radiographs using latent diffusion models for training thoracic abnormality classification systems, in: 2023 IEEE 20th International Symposium on Biomedical Imaging (ISBI), pp. 1–5.
- Paszke, A., Gross, S., Massa, F., Lerer, A., Bradbury, J., Chanan, G., Killeen, T., Lin, Z., Gimelshein, N., Antiga, L., Desmaison, A., Köpf, A., Yang, E., DeVito, Z., Raison, M., Tejani, A., Chilamkurthy, S., Steiner, B., Fang, L., Bai, J., Chintala, S., 2019. PyTorch: an imperative style, high-performance deep learning library, in: Proceedings of the 33rd International Conference on Neural Information Processing Systems, Curran Associates Inc., Red Hook, NY, USA. p. 721.
- Peng, J., Beetz, M., Banerjee, A., Chen, M., Grau, V., 2024. Generating virtual populations of 3D cardiac anatomies with Snowflake-Net, in: Statistical Atlases and Computational Models of the Heart. Regular and CMRxRecon Challenge Papers, Cham. pp. 163–173.
- Pinaya, W.H.L., Tudosi, P.D., Dafflon, J., Da Costa, P.F., Fernandez, V., Nachev, P., Ourselin, S., Cardoso, M.J., 2022. Brain imaging generation with latent diffusion models, in: Deep Generative Models, Cham. pp. 117–126.
- von Platen, P., Patil, S., Lozhkov, A., Cuenca, P., Lambert, N., Rasul, K., Davaadorj, M., Wolf, T., 2022. Diffusers: State-of-the-art diffusion models. <https://github.com/huggingface/diffusers>.
- Qin, C., Bai, W., Schlemper, J., Petersen, S.E., Piechnik, S.K., Neubauer, S., Rueckert, D., 2018. Joint learning of motion estimation and segmentation for cardiac MR image sequences, in: International Conference on Medical Image Computing and Computer-Assisted Intervention, pp. 472–480.
- Ramachandran, P., Zoph, B., Le, Q.V., 2018. Searching for activation functions, in: 6th International Conference on Learning Representations, ICLR2018.

- Rombach, R., Blattmann, A., Lorenz, D., Esser, P., Ommer, B., 2022. High-resolution image synthesis with latent diffusion models, in: 2022 IEEE/CVF Conference on Computer Vision and Pattern Recognition (CVPR), pp. 10674–10685.
- Saharia, C., Chan, W., Saxena, S., Li, L., Whang, J., Denton, E.L., Ghasemipour, K., Gontijo Lopes, R., Karagol Ayan, B., Salimans, T., Ho, J., Fleet, D.J., Norouzi, M., 2022. Photorealistic text-to-image diffusion models with deep language understanding, in: Advances in Neural Information Processing Systems, pp. 36479–36494.
- Schuhmann, C., Vencu, R., Beaumont, R., Kaczmarczyk, R., Mullis, C., Katta, A., Coombes, T., Jitsev, J., Komatsuzaki, A., 2021. LAION-400M: Open dataset of CLIP-filtered 400 million image-text pairs, in: Proceedings of the Data Centric AI NeurIPS Workshop 2021.
- Seale, T., Beetz, M., Rodriguez, B., Grau, V., Banerjee, A., 2024. Modelling multi-phase cardiac anatomy using point cloud variational autoencoders, in: 2024 IEEE International Symposium on Biomedical Imaging (ISBI), pp. 1–5.
- Suinesiaputra, A., Ablin, P., Albà, X., Alessandrini, M., Allen, J., Bai, W., Çimen, S., Claes, P., Cowan, B.R., D’hooge, J., Duchateau, N., Ehrhardt, J., Frangi, A.F., Gooya, A., Grau, V., Lekadir, K., Lu, A., Mukhopadhyay, A., Oksuz, I., Parajuli, N., Pennec, X., Pereañez, M., Pinto, C., Piras, P., Rohé, M.M., Rueckert, D., Säring, D., Sermesant, M., Siddiqi, K., Tabassian, M., Teresi, L., Tsaftaris, S.A., Wilms, M., Young, A.A., Zhang, X., Medrano-Gracia, P., 2017. Statistical shape modeling of the left ventricle: myocardial infarct classification challenge. *IEEE Journal of Biomedical and Health Informatics* 22, 503–515.
- Vincent, K.P., Forsch, N., Govil, S., Joblon, J.M., Omens, J.H., Perry, J.C., McCulloch, A.D., 2021. Atlas-based methods for efficient characterization of patient-specific ventricular activation patterns. *EP Europace* 23, i88–i95.
- Xu, H., Zacur, E., Schneider, J.E., Grau, V., 2019. Ventricle surface reconstruction from cardiac MR slices using deep learning, in: International Conference on Functional Imaging and Modeling of the Heart, pp. 342–351.
- Yang, G., Huang, X., Hao, Z., Liu, M.Y., Belongie, S., Hariharan, B., 2019. PointFlow: 3D point cloud generation with continuous normalizing flows, in: 2019 IEEE/CVF International Conference on Computer Vision (ICCV), pp. 4540–4549.
- Zhang, N., Yang, G., Gao, Z., Xu, C., Zhang, Y., Shi, R., Keegan, J., Xu, L., Zhang, H., Fan, Z., Firmin, D., 2019. Deep learning for diagnosis of chronic myocardial infarction on nonenhanced cardiac cine MRI. *Radiology* 291, 606–617.